



Cite this: *J. Anal. At. Spectrom.*, 2023, 38, 917

## High-speed and high-resolution 2D and 3D elemental imaging of corroded ancient glass by laser ablation-ICP-MS†

Roberta Zanini, <sup>ab</sup> Marco Roman, <sup>c</sup> Elti Cattaruzza <sup>b</sup> and Arianna Traviglia <sup>ab</sup>

In this work, laser ablation-inductively coupled plasma-mass spectrometry was used to investigate for the first time glass weathering mechanisms using high-resolution 2D and 3D elemental maps of altered layers of ancient glass. Roman archaeological glass shards, displaying several corrosion indicators, were studied using multiple raster-scanning ablation with high depth and lateral resolution. The concentration gradients of different elements were captured (in their variations from the surface to the bulk of pristine glass) by multiple ablations on degraded regions of interest to observe the dissolution of the glass network due to the hydration and leaching processes that occur during its alteration. The results indicated an enrichment of silicon and a depletion of alkaline/alkaline earth element concentration in the first few microns of depth under the surface area suggesting that a de-alkalinisation phenomenon occurs on the glass surface when ancient items have been buried under soil for extended timeframes. The layer-by-layer elemental distribution revealed also how the composition of the archaeological glass changes from the bulk to the surface, shedding light on the leaching behaviour of glass constituents during the alteration process.

Received 13th October 2022  
 Accepted 3rd February 2023

DOI: 10.1039/d2ja00337f  
 rsc.li/jaas

## 1 Introduction

In the study of glass corrosion, the reactions involved in the mechanism of alteration are mainly ascribed to the interaction between the glass surface and aqueous solutions. The phenomenon is normally described as follows. Initially, the surface of glass gets hydrated and the alkaline and alkaline-earth ions that are in the glass network are leached out and substituted with the hydrogen ions of the attacking solution. Afterwards, this ion-exchange process leads to an increase of hydroxyl group concentration in the solution resulting in a pH rise (above 9). From this, it follows that the chemical stability of glass is more susceptible to alkaline attack that promotes the dissolution of the glass network through the rupture of the Si-O bonds.<sup>1</sup> Although numerous published studies have addressed the topic of the interaction between glassy materials and the environment since the beginning of the last century,<sup>2–8</sup> the mechanism of glass corrosion is still largely unfamiliar to the chemistry community, and it has not been fully understood yet.

In particular, the great number of intrinsic and extrinsic factors involved in the process of glass alteration, such as the composition of glass itself, and the chemical and physical properties of the environment – temperature, pH, and especially the amount of water available – determine the rate and the kinetics of glass deterioration. Archaeological glass is often found in a poor state of conservation due to the burial conditions in which the archaeological items have been ageing for centuries. The degree of surface alteration can range from unperceivable to so heavily degraded that the original aspect of the glass is no longer perceptible because of its complete transformation into corrosion products. The partial or total physicochemical transformation of archaeological glass can induce a variety of alteration marks that are optically observable on its surface, such as iridescence, discolouration, pitting, and cracking.<sup>9</sup> Often, one or more of these visible manifestations of deterioration can simultaneously develop across the surface of a glass artefact. In the majority of the cases, the investigation of the chemical composition of the ancient glass surface and its morphology, of the degradation pathologies that affect it, and of the corrosion products deposited on it is carried out using conventional techniques such as X-ray fluorescence (XRF) spectroscopy,<sup>10</sup> optical or scanning electron microscopy (SEM),<sup>11</sup> and Raman spectroscopy.<sup>12</sup> Portable XRF spectrometers are typically used for *in situ* characterisation of glass museum collection, but the failure of this technique to monitor Na concentration limits its application for studying corrosion, with Na being one of the main elements involved in the leaching process during glass

<sup>a</sup>Center for Cultural Heritage Technology, Istituto Italiano di Tecnologia, Via Torino 155, Venezia-Mestre, Italy. E-mail: roberta.zanini@iit.it; arianna.traviglia@iit.it

<sup>b</sup>Department of Molecular Sciences and Nanosystems, Ca' Foscari University of Venice, Via Torino 155, Venezia-Mestre, Italy

<sup>c</sup>Department of Environmental Sciences, Informatics and Statistics, Ca' Foscari University of Venice, Via Torino 155, Venezia-Mestre, Italy

† Electronic supplementary information (ESI) available. See DOI: <https://doi.org/10.1039/d2ja00337f>



alteration. SEM coupled to energy dispersive X-ray (EDX) spectroscopy allows the chemical characterisation of ancient glass, but data collection is limited to the first microns of depth. In addition, both SEM and XRF techniques provide only semi-quantitative data.<sup>13</sup> Raman spectroscopy, instead, is a suitable non-destructive technique to obtain qualitative information about glass samples. The small laser spot size ( $>1 \mu\text{m}$ )<sup>14</sup> generated using the  $\mu$ -Raman technique enables a very punctual analysis, but this represents a limit when analysing degraded glass that presents a heterogeneous aspect on the scale of hundreds of microns. Overall, these techniques have several limitations when examining corroded glass since the alteration phenomenon, which often involves a considerable thickness of the glass surface and leads to a heavy chemical and physical transformation of it, requires high but adjustable in-depth and lateral resolution investigation. LA-ICP-MS, instead, can overcome some of these shortcomings. While being a well-established analytical technique for the characterisation of ancient glass,<sup>15–17</sup> its use remains mostly limited to obtaining the bulk chemical composition of the (unaltered) substrate, whereas published studies in which this technique is used to specifically study the surface degradation are scarce.<sup>18–20</sup> LA-ICP-MS analysis is based on the direct micro sampling of a solid volume and the subsequent elemental analysis of the generated material *via* a mass spectrometry detector. It is considered a “quasi” non-destructive (or micro-destructive) technique, requiring minimal or no sample preparation, while providing higher sensitivity/lower detection limits (in the  $\text{ng g}^{-1}$  range) compared to more conventional techniques used for glass characterisation.<sup>13,21,22</sup> In addition, it enables full quantitative determination of major, minor, and trace elements within a single analytical run. All these properties make LA-ICP-MS suitable for performing bulk chemical characterization of ancient glass, which provides information about the provenience of raw materials used for glass manufacturing (sands, fluxes, and chromophores), or about fabrication technologies, which vary widely according to the historical period and/or geographical area.<sup>23–25</sup> For example, multi-elemental mapping of polychrome glass artefacts collected using the LA-ICP-MS rastering procedure analysis can provide information about the distribution of different colouring agents used to produce a particular colour and consequently elucidate about the manufacturing of decorated ancient glass artefacts.<sup>26</sup> Besides, the opportunity to deeply investigate the surface in an adjustable way enables the gathering of data about the changes in the chemical composition of ancient glass with an in-depth resolution of about 150 nm.<sup>19</sup> This type of information is valuable not only to address archaeological and historical questions, but also to provide insights to be used for conservation and restoration purposes. The LA-ICP-MS analysis of a solid sample can be performed using the single spot mode or using the line scanning mode where the sample is moved at a constant speed while being under ablation. Both modes can potentially be applied in a raster framework to generate 2D elemental maps, and in multiple per-point ablations to generate 3D maps. To achieve the goal of characterising archaeological altered glass samples in greater detail, our work defined a novel methodology

to achieve high-quality and high-speed 2D and 3D elemental mapping of ancient glass moving from a tested fine-tuning protocol developed by Van Elteren *et al.*<sup>27</sup> which uses fast aerosol transport technology and high-repetition rate.<sup>28</sup> This protocol has been originally developed and validated for 2D imaging using a modern ‘murrina glass’ (a piece of cut reed) from Murano (Venice), an ideal sample in that it offers a flat and homogeneous surface.<sup>29</sup> In our work, Van Elteren *et al.*’s protocol has been optimised, expanded to the 3<sup>rd</sup> dimension (depth) and applied to real samples of historical interest, obtaining high-quality images and the opportunity to perform innovative and comprehensive characterisation of the corrosion layers of archaeological glass. This study reports a set-up approach for LA-ICP-MS analysis to achieve 2D and 3D elemental imaging of heavily degraded archaeological glass by retrieving information on the lateral and in-depth distribution of elements that is pivotal for a more complete investigation of the corrosion mechanism of ancient glass. The obtained results demonstrate how LA-ICP-MS can be successfully used to investigate the deterioration features that get formed on archaeological glass: this represents a great opportunity to study and better understand the processes involved in glass corrosion in the long term. If correctly analysed, the chemical and structural transformation of ancient glass makes available to the scientific community information relative to a very extended time span (in terms of millennia) that can be hardly gathered in alternative ways.

## 2 Materials and methods

Optimised LA-ICP-MS imaging methods have been used in this work to analyse Roman glass shards that have been recovered from topsoil during fieldwalking surveys in Aquileia (NE Italy), having surfaced from their buried stratigraphic context after centuries due to ploughing.<sup>30</sup> The samples date between the 1<sup>st</sup> and the 4<sup>th</sup> century BC, and they have a silica–soda–lime composition typical of the glass production during those years. These shards show different types of degradation including pits, cracks, dark deposition, and iridescent patina. The glass fragments analysed were selected based on both size and sufficiently regular and flat surface to avoid resin mounting or sub-sampling. The samples were cleaned with water as soon as they were picked up from the soil during the survey campaign, but no organic solvent was used to clean the samples, nor they were polished before performing the analysis. Pre-ablation was not performed in order to preserve all the valuable information about the glass surface composition, which maintains traces of all the effects determined by the environment triggering natural glass alteration. Data on possible contamination of the surface due to the interaction between the glass surface and the burial environment would be also retained as they can provide further relevant information. The choice not to perform pre-ablation and the connected advantages and limitations are specifically discussed in the following sections of this paper. The LA-ICP-MS instrument used in this research consists of an Analyte Excite ArF excimer 193 nm laser (Teledyne CETAC Photon Machines) coupled to an iCAP-RQ quadrupole ICP-MS (Thermo



Scientific). The laser ablation device is equipped with a HelEx II two-volume ablation cell mounted on a high-precision xy translating stage. The samples were placed on a standard LA holder and fixed in-place with double-sided tape. A rapid aerosol transfer line (ARIS, Teledyne CETAC Technologies) and helium as carrier gas were used to transport the ablated materials from the surface of the sample to the ICP-MS. The use of ARIS enables achieving a faster washout time (WOT), typically in the range of 20 ms, specifically designed for high-speed imaging. Being applied to weathered glass analysis, the WOT was calculated using the certified reference material (CRM) NIST 612 as reference, since the glass samples had a heterogeneous and unknown surface composition, resulting in larger but unsystematic WOT (see Section 3.1). The maps were obtained using a monodirectional scan mode with a  $20 \times 20 \mu\text{m}^2$  square spot size, a laser fluence of  $4 \text{ J cm}^{-2}$ , and a fixed dosage of 7. Three-dimensional elemental maps were obtained by repeated ablation of the same region of interest (ROI) under the same operating conditions. Each data file for 3D image generation was acquired and saved individually as a .csv file, to be then stacked in the processing phase. This enabled consistent monitoring of both the elemental composition of a single ablated layer or the 3D volume distribution of elements. The LA-ICP-MS operating parameters were adapted according to the approach reported by Van Elteren *et al.*,<sup>31</sup> which is a setup for high-speed imaging without artefacts. Once calculated the WOT and preselected the dosage and the spot size, the laser repetition rate (Hz) was fixed to  $1000 \times$  dosage/washout time, while the resulting scan speed equaled [(spot size)/

(washout time/1000)]. A repetition rate of 280 Hz corresponding to  $800 \mu\text{m s}^{-1}$  of scanning speed, considerably faster than that set up in the previous study of LA-ICP-MS glass imaging,<sup>26</sup> was adopted. In addition, the selection of a higher dosage enabled the generation of each pixel based on multiple – partially overlapping – laser pulses that improve the signal-to-noise ratio and the image quality, especially when a smaller spot size is used and multi elements are determined. Such a fast laser frequency required fast aerosol transport (achieved using the ARIS), but also accurate synchronisation with the ICPMS acquisition method. The use of a quadrupole (sequential) mass analyser forced to select a small group of analytes/isotopes to be monitored within a total sweep time equivalent to the WOT. The elements of interest were selected based on preliminary line scanning of the surface nearby the ROI. Based on the same preliminary data, the individual dwell time of selected isotopes was adjusted to be inversely proportional to their expected signal intensity (concentration). Six elements/isotopes were routinely recorded per image, depending on the specific glass sample composition, choosing among  $^{23}\text{Na}$ ,  $^{27}\text{Al}$ ,  $^{29}\text{Si}$ ,  $^{39}\text{K}$ ,  $^{43}\text{Ca}$ ,  $^{55}\text{Mn}$ ,  $^{57}\text{Fe}$ , and  $^{59}\text{Co}$ . The LA-ICP-MS operating parameters are summarised in Table 1.

This setup considered high dosage, high-repetition lasing mode and fast WOT as the optimal operating conditions to obtain fast mapping and avoid aliasing and other image artefacts. The data elaboration steps (including background subtraction, drift correction, image reconstruction and quantitative calibration) were performed using the software HDIP (Teledyne Photon Machines, Bozeman, MT, USA). The elemental maps generated by HDIP based on raw signal intensity data (expressed in counts per seconds) were first converted into mass concentration maps by applying a calibration curve obtained from the analysis of a set of standard reference materials. Eight reference materials were used for LA-ICP-MS calibration: (i) Corning Museum of Glass synthetic glass standard materials A, B, C, and D, replicating the composition of ancient glass; (ii) Society of Glass Technology glass standards 7, 10, and 11; and (iii) NIST SRM glass 612. The latter was used also for signal drift correction throughout the ablation. Linear scans on each reference glass were carried out before (and after in the case of NIST SRM 612) the acquisition of each map. Before the map generation, elemental concentrations determined were transformed into the corresponding oxide concentrations according to the conventional approach.<sup>19</sup> For each ablated layer independently, the oxide concentration was finally normalised by making the 98<sup>th</sup> percentiles of all the determined oxides sum to 100%. The purpose of the normalisation was to obtain consistently viewable and comparable maps layer-by-layer. We have adopted standard calibration and normalisation parameters considering the components of glass samples as oxides and thus obtaining a consistent scale for all the ablated layers. However, since corroded glass is not only composed of oxides, this method should not be understood as an unambiguous chemical and mineralogical interpretation of the components that are normally present on archaeological glass.

Table 1 Operating parameters of the LA-ICP-MS 2D and 3D imaging of weathered ancient glasses

Laser	
Laser type	ArF excimer 193 nm
He gas flow cell	$0.25 \text{ L min}^{-1}$
He gas flow cup	$0.25 \text{ L min}^{-1}$
Transfer line	ARIS
Fluence	$4.0 \text{ J cm}^{-2}$
Spot size	$20 \mu\text{m}$ square
Washout time	20 ms
Ablation mode	Fixed dosage (7)
Repetition rate	280 Hz
Scanning mode	Monodirectional raster
ICP-MS	
RF power	1550 W
Cooling gas flow	$14 \text{ L min}^{-1}$
Auxiliary gas flow	$0.8 \text{ L min}^{-1}$
Ar makeup gas flow	$0.8 \text{ L min}^{-1}$
Monitored isotope masses (a max of 6 per run)	$^{23}\text{Na}$ $^{27}\text{Al}$ $^{29}\text{Si}$ $^{39}\text{K}$ $^{43}\text{Ca}$ $^{55}\text{Mn}$ $^{57}\text{Fe}$ $^{59}\text{Co}$
Total sweep time (duty cycle)	20 ms (60%)



### 3 Results and discussion

#### 3.1 Improved impurity imaging on ancient glass by LA-ICPMS

According to one of the pioneering studies about 2D LA-ICP-MS elemental imaging,<sup>29</sup> a correct selection of optimal acquisition conditions (such as laser beam size, scanning speed, repetition rate, and washout/dwell time) is pivotal to achieve fast high-resolution analysis with minimal image degradation in terms of blur, aliasing, smear, and noise. Maintaining a consistent synchronisation between LA and ICP-MS parameters, in particular, is essential to avoid the occurrence of aliasing and interference patterns. In previous applications of LA-ICP-MS for studying glass corrosion phenomena, 3D elemental maps of weathered glass were obtained by employing a drilling procedure based on 50 laser pulses per grid point at a pulse rate of 1 Hz.<sup>19</sup> The authors asserted that the tested procedure limits element fractionation and re-ablation of the earlier deposited material on the ablation crater walls or surface. These are the commonly encountered problems that occur in deep craters due to the reduction of ablated mass per pulse and/or ineffective transport of aerosolized particles at increasing depth, both resulting in the decay of signal intensities with time, and possibly elemental fractionation.<sup>32</sup> A detailed comparison between the previous and our proposed LA-ICP-MS imaging approach points out the differences and advantages in the laser system optimisation, in particular as far as the scanning mode analysis is concerned. The choice of using a square laser spot and a mono-directional, continuous scanning mode – instead of using a drilling mode procedure with a circular laser spot – gives a more complete regional coverage (Fig. 1) providing more representative chemical characterisation of the whole ROI. The heterogeneous aspect of corroded samples at the micro-scale (see the alteration pits in Fig. 4), smaller than the spot size used in the previous work (diameter of 80  $\mu\text{m}$ ),<sup>19</sup> shows that it is crucial to cover completely the area of analysis and reap a quantitative data that is representative of the entire surface. In addition, the spatially continuous ablation of all the ROI minimises the probability to fall into elemental fractionation issues due to the proximity of the crater walls, as in the case of Fig. 1a.

The use of a smaller laser beam spot size (20  $\mu\text{m}$ ) proved to be pivotal for clearly defining some morphological details of glass alteration present on the surface – or below it – improving the image resolution. By operating in a rastering mode, it is also

possible to continuously ablate the material up to greater depths into the sample (a few microns) without encountering edge effects and signal decrease. In addition, it has been demonstrated that overlapping laser pulses (dosage > 1) are preferable to obtain high quality images in multi elemental imaging.<sup>28</sup> Recent developments in the optimisation of the LA-ICP-MS imaging setup have established that a high repetition rate laser system and fast washout time are key conditions to achieve “fast LA-ICP-MS analysis with excellent image quality”.<sup>27,28</sup> The LA-system equipped with the ARIS enables achieving very low WOT. In this study, the WOT is calculated daily based on the ablation of the certified reference material CRM NIST 612, instead of the archaeological sample object of the study. This choice was based on the altered archaeological glass sample heterogeneity, as its surface morphology makes the robust WOT evaluation virtually impossible, given that it requires a stable and repeatable signal, which is impossible to obtain by ablating a contiguous area on the real corroded sample. A feasible solution may be to quantify the WOT on different areas of the sample, but the estimate would not be sufficiently robust, in any case, considering that the scan would involve heterogeneous areas of the sample. In addition, the latter strategy results in multiple region-specific WOTs that implicate a challenging assessment of which is the best to use. The WOT value resulting from NIST SRM 612 is more representative of the instrumental configuration/status than of the specific sample to be analysed, but this approach can be trusted to obtain high quality images without artefacts from real samples (as visible in the following Fig. 3–5). To better explain the motivations that led us to make this choice, Fig. 2 represents a synthesis of WOT measurements based on monitoring  $^{43}\text{Ca}$  on NIST 612 and an archaeological glass sample using a 20  $\mu\text{m}$  square spot size. Comparing the repeatability of peak width, the necessity of using NIST 612 to achieve a systematically reliable estimate of the WOT is evident.

Once the WOT was evaluated, the dwell time (ms) was optimised for each element individually and for each sample specifically, to be inversely proportional to the expected spatial average of signal intensity (*i.e.* elemental concentration, based on a preliminary quick measurement) and constrained to a total dwell time equal to the WOT (20 ms). In Van Elteren *et al.* work,<sup>19</sup> all of the elements were instead acquired at a fixed dwell time of 1 ms without considering their different concentrations in the glass matrix. It should be noted that a fast scanning speed and washout time in the ms range limit the number of elements that can be determined by using a sequential detector mass analyser such as the quadrupole MS;<sup>27</sup> in this work six elements were monitored within a single run. The published 3D LA-ICP-MS mapping for studying the weathering phenomena using a drilling procedure reports that 19 isotopes including major, minor, and trace elements were acquired. Still, only Si, Mg, and Mn were discussed as representative for three corresponding types of leaching mechanism, showing that fewer but carefully selected elements could still provide all significant information. Investing in map quality (absence of artefacts, resolution, size and spatial representation of the ROI) appears to be a richer

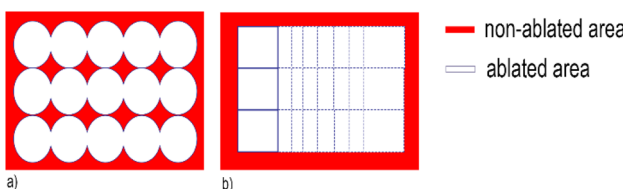


Fig. 1 (a) Drilling mode with the circular spot size procedure used;<sup>19</sup> (b) continuous scanning mode with the square spot size procedure used in the present work.



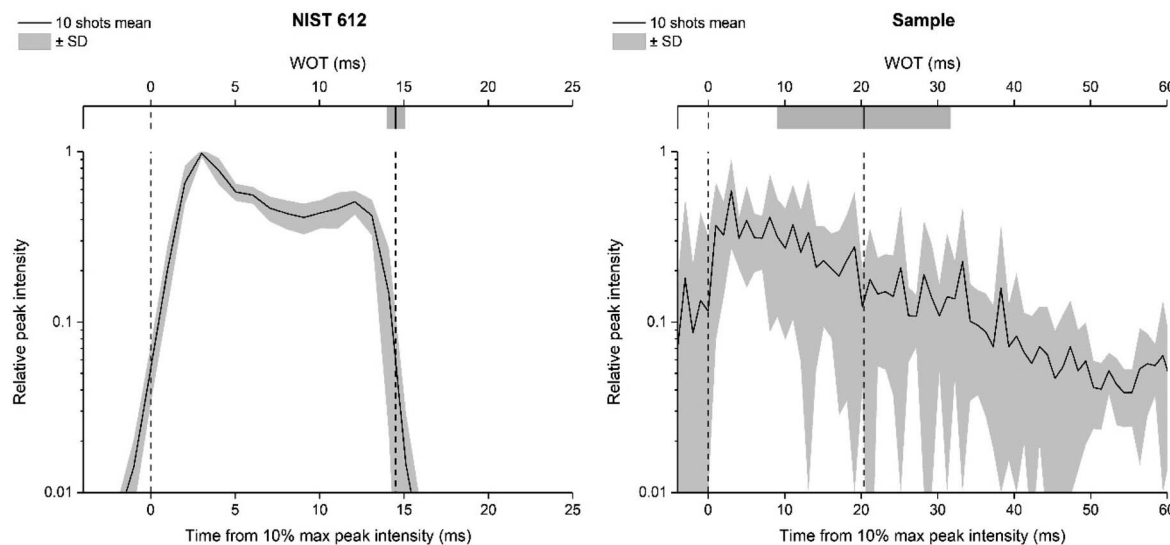


Fig. 2 Example of single shot peak profiles for WOT calculation based on NIST 612 and the real sample: mean of 10 consecutive shots  $\pm$  standard deviation (SD). The results in WOTs are  $14.5 \pm 0.5$  ms for NIST and  $20 \pm 11$  ms for the sample.

strategy for the study of the alteration mechanisms of archaeological glass using 2D and 3D elemental imaging.

### 3.2 Procedure application on archaeological degraded glass

The analytical method described in the previous section has been applied for the characterisation of Roman glass samples that exhibited different types of alteration: cracking, pitting, and the formation of iridescent patina. Fig. 3 shows the element distribution in a cracked glass sample. This unique type of glass alteration is quite rare and there is little published information about similar groove formation on archaeological glass.<sup>33</sup> A recently published article<sup>34</sup> has proposed a theoretical explanation of the U/V-groove formation and propagation on tektite

glass, which is, like all glass, subjected to weathering. Its authors stated in the paper that the formation and propagation of cracks is controlled by internal tensile stresses and by the corrosion rate. Based on this assumption, the authors suggested that extensive studies should be performed to understand the phenomenon of crack development considering all potential factors involved, such as the pH, humidity, porosity, and permeability of the soil. Here, the used beam spot size of  $20 \mu\text{m}$  allows us to pinpoint sharp boundaries between the composition of the glass matrix and that of the cracks, as clearly shown by the comparison of Na and Al distribution (Fig. 3d). The cracks, which extend throughout the entire sample, seem to be filled by the mineralised material acting as a cement. The presence of Si, Ca, and high levels of Al and K in the cracks

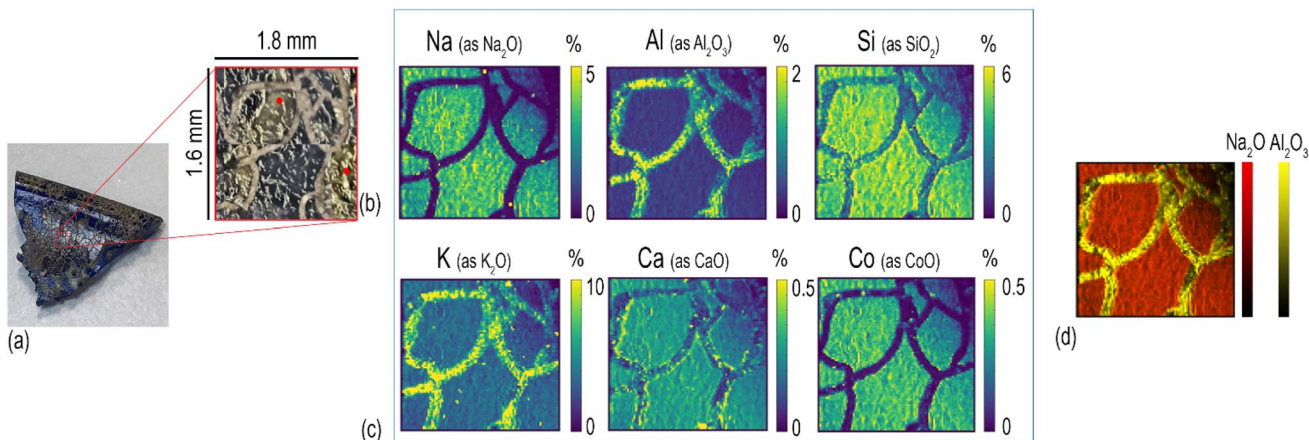


Fig. 3 (a) Roman archaeological glass fragment found in Aquileia area (NE Italy); (b) a mosaic of images of the ablated area; (c) elemental Na, Al, Si, K, Ca, and Co concentrations, conventionally expressed as the normalized level of their respective oxides in % by weight; (d) overlay distribution of Na and Al in the same area of analysis. Lateral resolution  $20 \mu\text{m}$ . The 2D elemental maps of the cracked sample show a decrease of the intensity at the top right for all the monitored elements due to the focus loss in this area. Concentrations are conventionally reported as oxides normalised to 100 for consistent visualisation purposes between layers but should not be understood as the actual mineralogical/chemical composition of the sample (see the Materials and methods section).

(Fig. 3c) suggests that this filler might be related to the soil in which the sample aged – buried – for centuries. Calcium appears to accumulate mainly along the edges of glass fragments and its concentration on the glassy parts of the sample is unexpectedly low considering that the archaeological sample is expected to have a significant level of CaO as a stabiliser, being a soda–silica–lime Roman glass. The formation of cracks could be the consequence of a low Ca concentration in the glass matrix, with such element being the main factor that determines the degree of degradation of glass in soil burial conditions.<sup>35</sup> The low level of Ca in the glass network causes the leaching of Na and the formation of a surface altered layer that is continuously exposed to drying and wetting cycles due to the action of seasonality and soil conditions (pH, salt concentration, and permeability). During such cycles, the glass shrinks and expands, causing mechanical stress at the interface

between the pristine glass and the altered layer, resulting finally in the formation of cracks. The blue colour of this glass fragment is determined by the colouring agent Co<sup>2+</sup>, which is exclusively present in the glassy parts of the sample (Fig. 3c), resembling the distribution of Na. The concentration of Co is uniform over the entire surface of the sample even though it is possible to observe whitish zones in the ablated area (indicated in Fig. 3b with a red dot).

Element distribution maps were obtained through the layer by-layer ablation of the same ROI; each data file was then individually saved and elaborated using HDIP and MatLab. Fig. 4 shows the in-depth element distribution in an archaeological Roman glass sample where the corrosion phenomenon is represented by the presence of scattered pits. The ablation was performed ten times on the same area of this sample, resulting in ten maps corresponding to different layers and

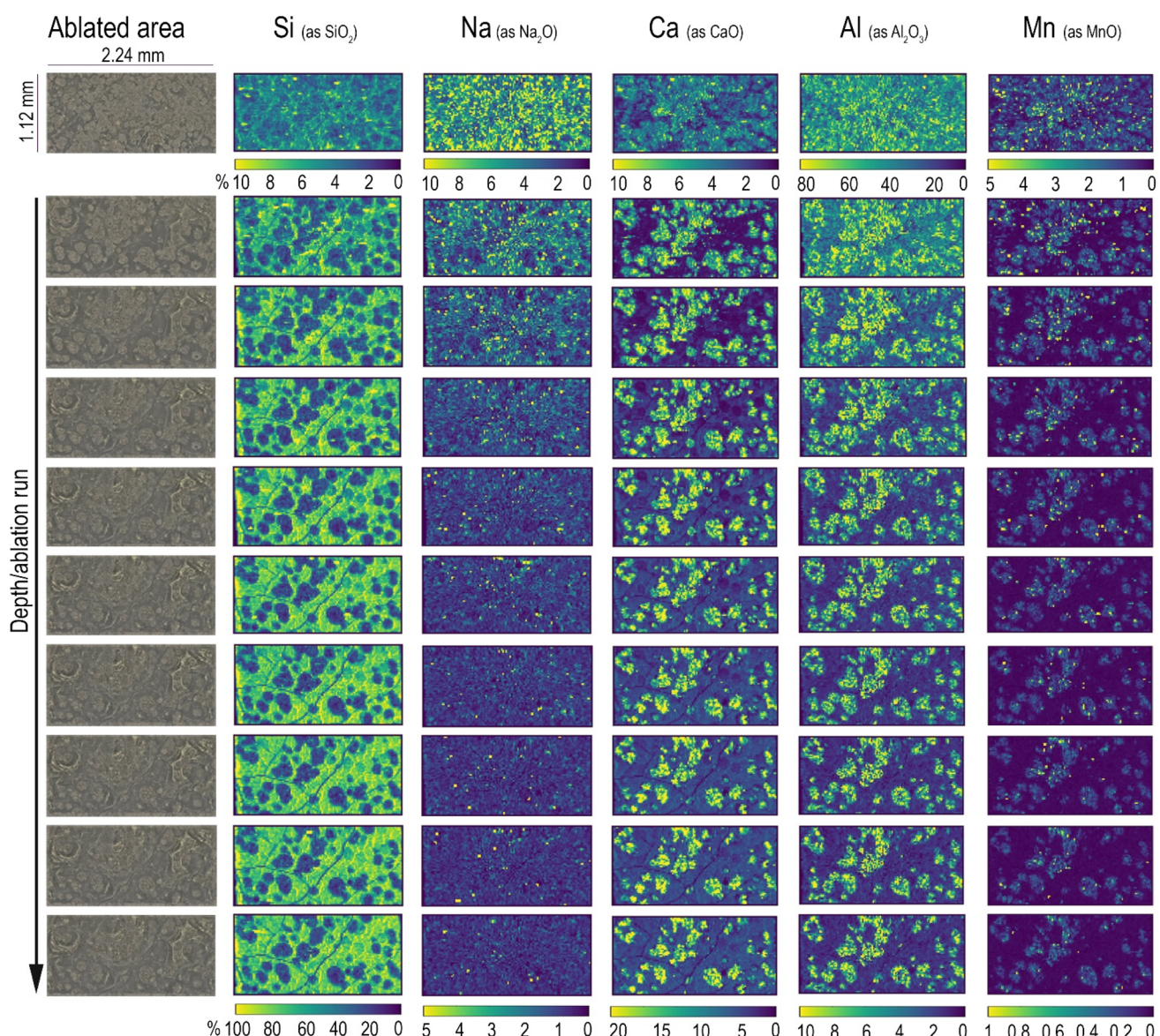


Fig. 4 2D element distribution of the exploded 3D maps of Si, Na, Ca, Al, and Mn distributions, conventionally expressed as the normalized level of their respective oxides in % of mass, in an archaeological glass sample showing pitting corrosion. Lateral resolution 20  $\mu$ m.



showing the overall distribution of the monitored elements from the surface to the bulk of the sample. The maps display that Ca, Mn, and Al are accumulated into the pits, a phenomenon likely due to the deposition of soil minerals. Conversely, Si is mostly concentrated in the glassy areas of the sample. In particular, starting from the second layer ablated from the surface, the Si maps point out several cracks that are not visible to the naked eye due to the deposition of soil material on the glass surface. This evidence is congruent with a deterioration of the vitreous material in burial conditions as reported by a study of Palomar *et al.*<sup>36</sup> who investigated glass corrosion using a model extracted from historical glass under simulated burial conditions. This latter study described the appearance of cracks on the surface of the glass as one of the first steps of the alteration that affects typical Roman glass. Such cracks grow later in pits that became interconnected during advanced corrosion stages. The concentration of elements in the top layer of the glass appears completely different from those of in the glass bulk. In particular, the amount of Al on the surface is eight times higher compared to what is found from the second ablated layer onward, and, in contrast, the concentration of Si in the surface is considerably lower than that monitored in the glass bulk (Fig. 4). These superficial element concentrations in the sample surface suggest that the soil and moist material directly in contact with the surface of the sample for centuries have strongly contaminated it. Generally, when LAICP-MS is used to analyse the ancient glass, pre-ablation is performed to remove potential surface contaminants prior to the analysis.<sup>37-39</sup> Here, instead, the objective was to characterise a specific glass alteration at the very surface level. Thus, pre-ablation of the specimen was avoided to preserve the chemical information coming from the top layer, which can be considered as the interface between the glassy material and the surrounding environment.<sup>22</sup> Inevitably, this implies the need for special care in the interpretation of the top layer and the potential contamination derived from burial conditions should be carefully taken into account (Fig. 4). With similar concerns in mind, preliminary cleaning of the specimen should be done in a very cautious way, not to affect the surface of the artefact, and manual polishing should be avoided. These operations could, as a matter of fact, result in uneven topographical features to which laser irradiation conditions (*e.g.*, focus) can be very limitedly adapted within a single ablation run (layer map) and could further complicate a situation made potentially complex also from the original morphology and surface structure of the sampled object. An accurate selection of ROIs is therefore key to a successful analysis. The maps of the layers from the second to the tenth illustrate, instead, the concentration of the elements on the glassy material and its structural diversity. The 2D element distribution indicates an increase of Si, Al, and Na concentration in the first few nanometres under the surface area. This distribution could be the result of a process of cation leaching during the initial stage of glass corrosion when the glass object was buried in soil.<sup>40</sup> The lower concentration of Si inside the pits is, instead, linked to the process of their formation. During the alteration process in alkaline conditions, the dissolution of the glass network is the predominant

deterioration mechanism, when isolated fissures appear on the surface of the glass (like those visible on the Si maps in Fig. 4) due to the dissolution of Si–O–Si bonds. Subsequently, the prolonged exposure of the glass surface to the soil causes an increase of the attacking solution pH, involving the formation of basic species ( $\text{OH}^-$ ) that progressively break the Si–O–Si bonds. This causes the widening of the fissures and, ultimately, the formation of pits as a result of the local dissolution of the glass network.<sup>41</sup> As for the previously described glass analysis (Fig. 3), also in this case the sharp concentration gradients between the glassy surface and the pits composition were seen using a small spot size (20  $\mu\text{m}$ ), as shown in Fig. 4.

Another visible effect of degradation, which is most commonly found on glass recovered from archaeological excavation sites, where it has been aging under soil, is iridescence.<sup>9</sup> This is caused by changes in the composition of the surface of weathered glass due to the interaction of the object with soil elements in direct contact, often resulting in the disintegration and flaking of the glass surface. Generally, archaeological glass is characterised by a metallic aspect resulting from the formation of a multi-layer patina (with empty spaces between one layer and the other filled with air) which determines a rainbow-like effect due to the reflection of light. This type of glass alteration has been investigated in this work by observing the elemental distribution in a remarkably iridescent Roman glass sample.

The area selected for the analysis of this sample was ablated ten times for monitoring six elements: Si, Na, Ca, Al, Mn, and Co. Fig. 5 shows the changes in element concentration profiles looking at their distribution starting from the surface and going to the bulk of the glassy matrix. Three main types of leaching mechanisms can be identified by observing the depth profiles related to  $\text{SiO}_2$  (network former), to  $\text{Na}_2\text{O}$  (network modifier) and to  $\text{Co}^{2+}$  (heavy metal present in the glass composition as a colouring agent). Starting from the surface, the first to be identified is a layer mainly composed of Si (Fig. 5). Silica, as a network former, appears to be relatively concentrated on the surface of the glass sample due to the solubilisation and depletion of alkali and alkaline-earth ions, while hydrated silica gel forms and accumulates on the surface of altered glass, often composed of a multi-layer structure. A recent study has analytically demonstrated that this laminated alteration, with a thickness ranging between 0.1 and 10  $\mu\text{m}$ , consists of a random packing of amorphous silica nanoparticles and it can be considered as one of the by-products of the leaching process that occurs in an alkaline environment.<sup>42</sup> The depth distributions of Na and Ca demonstrate a completely different leaching behaviour. The map of Na, which represents one of the most mobile elements in soda-silica-lime glass, shows that the concentration of alkaline elements decreases moving from the bulk to the surface. The top layer shows the presence of Na in the most iridescent area of the altered surface. Conversely, deeper ablation layers show an increase in Na concentration in the bulk of the sample, which appears more and more homogeneous in the deepest layer. This depth distribution reflects the depletion of sodium in the altered surface layers due to the leaching process, which is more likely to occur for smaller ions



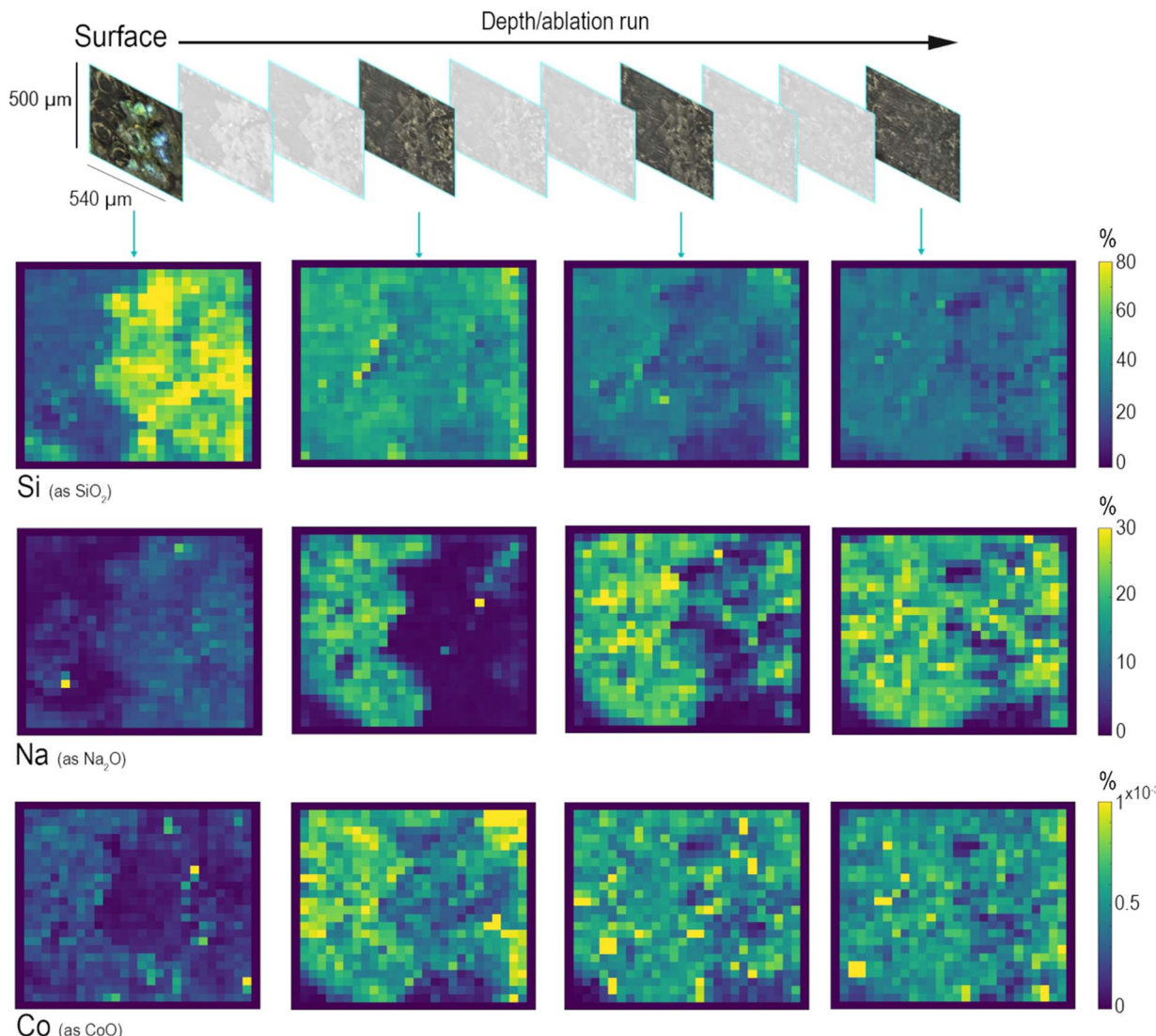


Fig. 5 2D element distribution of the exploded 3D maps of Si, Na, and Co distributions, conventionally expressed as the normalized level of their respective oxides in % of mass, in an archaeological glass sample that presents iridescent patina on the surface. Lateral resolution 20  $\mu\text{m}$ .

such as  $\text{Na}^+$ . Similarly, the distribution of Co shows the reduction of its concentration on the top layers, but the depth of depletion of these elements is less than that of Na. This difference in their distribution could be explained considering the classic theory of glass corrosion, which suggests that the preferential dissolution of more soluble cations happens during the initial part of the leaching process. Since each modifier cation has different diffusion coefficients, their diffusion through the glass network changes, depending on their size and charge, and on the composition of glass itself.<sup>5</sup> The maps of Fig. 5 show that the process of glass alteration must have occurred because of ion depletion, both alkaline ions ( $\text{Na}^+$ ) and heavy metal ions ( $\text{Co}^{2+}$ ). These results are the evidence of element distribution as a result of a dealkalination process that acted as a phenomenon occurring at the surface level while the glass item was buried in soil, showing how the composition changes from the bulk to the surface of the glass, and providing information about the corrosion mechanism.<sup>43</sup>

## 4 Conclusion and future perspective

In investigating Roman glass that has been lying underground for over 2000 years, the outcomes of this research offer insights used to trace back the transformation of the vitreous structure of ancient glass specimens and to correlate it to the natural mechanism of glass deterioration. This work also provides evidence of the intrinsic effectiveness of multi-elemental LA-ICP-MS analysis to investigate the process of glass corrosion. The possibility to look closely at the layer-by-layer elemental distribution – variations going from the bulk to the surface of the samples – provides the chance to observe how the composition of glass metamorphoses, exposing novel information about the progression of the corrosion phenomenon. We have now the means to state that the formation of an iridescent patina derives from a combined effect of the local presence of water and the composition of glass that determines the diffusion of ionic species from the external layers and the



consequent re-precipitation of hydrated silica and other alkali-derived compounds. This approach offers significant improvements compared to current state-of-the-art in terms of lateral and depth resolution and of image quality. The obtained results provide, thus, promising foundation for further investigation of different phenomena of alteration that affect archaeological and historical glass. Additional studies are ongoing with the aim of decreasing the spot size of the laser beam to reach higher lateral resolution with the goal of investigating other related phenomena of glass alteration that are still not completely known or understood (*i.e.*, the formation of rings). Future planned tests will also entail the characterisation of glass fragments from various chronological phases, which will give the opportunity to study alteration mechanisms (*e.g.*, crizzling) occurring in ancient glass with a bulk composition different from the Roman's one. In turn, the generated information will be used as background knowledge for the development of novel consolidation and preservation strategies for ancient glass, a very challenging area of research because of the amorphous nature of glass and its chemical and physical properties that can be affected and modified by intrinsic and extrinsic factors.

## Conflicts of interest

There are no conflicts to declare.

## Acknowledgements

The authors take the opportunity to thank the Museo Archeologico Nazionale di Aquileia and Soprintendenza Archeologia, Belle Arti e Paesaggio del Friuli-Venezia Giulia – Superintendency for Archaeology, Fine Arts and Landscape of Friuli – Venezia Giulia Region (Dr S. Bonomi and Dr P. Ventura) for research permissions.

## Notes and references

- 1 S. Davison, *Conservation and Restoration of Glass/Sandra Davison*, 2nd edn, 2006.
- 2 G. W. Morey, *Ind. Eng. Chem.*, 1925, **17**, 389–392.
- 3 R. J. Charles, *J. Appl. Phys.*, 1958, **29**, 1549.
- 4 A. Lavoiser, *Acad. Sci.*, 1770, **73**, 90.
- 5 R. Doremus, *Glass Surfaces*, 1975, vol. 19, 137–144.
- 6 W. B. White, *Corrosion of Glass, Ceramics and Ceramic Superconductors*, 1992, vol. 2–28.
- 7 R. Hellmann, S. Cotte, E. Cadel, S. Malladi, L. S. Karlsson, S. Lozano-Perez, M. Cabié and A. Seyeux, *Nat. Mater.*, 2015, **14**, 307–311.
- 8 C. Cailleteau, F. Angeli, F. Devreux, S. Gin, J. Jestin, P. Jollivet and O. Spalla, *Nat. Mater.*, 2008, **7**, 978–983.
- 9 N. A. R. van Giffen and S. P. Koob, *The Encyclopedia of Archaeological Sciences*, 2018, vol. 1–4.
- 10 G. Nuyts, S. Cagnò, K. Hellemans, G. Veronesi, M. Cotte and K. Janssens, *Procedia Chem.*, 2013, **8**, 239–247.
- 11 P. Bellendorf, H. Roemich, S. Gerlach, P. Mottner, E. López and K. Wittstadt, *Glass and Ceramics Conservation 2010: Interim Meeting of the ICOM-CC Working Group*, Corning, New York, U.S.A., 2010, pp. 137–144.
- 12 B. Hruška, A. Nowicka, M. Chromčíková, E. Greiner-Wrona, J. Smolík, V. Soltézs and M. Liška, *Int. J. Appl. Glass Sci.*, 2021, **12**, 613–620.
- 13 K. Janssens, *Modern Methods for Analysing Archaeological and Historical Glass, Volume I*, 2013, vol. 1.
- 14 I. A. Balakhnina, N. N. Brandt, A. Y. Chikishev, A. A. Mankova, E. A. Morozova, I. G. Shpachenko, V. A. Yuryev and T. V. Yuryeva, *J. Raman Spectr.*, 2018, **49**, 506–512.
- 15 P. Robertshaw, M. Wood, A. Haour, K. Karklins and H. Neff, *J. Archaeol. Sci.*, 2014, **41**, 591–604.
- 16 J. Varberg, B. Gratuze and F. Kaul, *J. Archaeol. Sci.*, 2015, **54**, 168–181.
- 17 H. Walder, *Midcont. J. Archaeol.*, 2013, **38**, 119–142.
- 18 S. Panighello, J. T. Van Elteren, E. F. Orsega and L. M. Moretto, *Anal. Bioanal. Chem.*, 2015, **407**, 3377–3391.
- 19 J. T. Van Elteren, A. Izmer, M. Šala, E. F. Orsega, V. S. Šelih, S. Panighello and F. Vanhaecke, *J. Anal. At. Spectrom.*, 2013, **28**, 994–1004.
- 20 L. Dussubieux, P. Robertshaw and M. D. Glascock, *Int. J. Mass Spectrom.*, 2009, **284**, 152–161.
- 21 M. Guillong and D. Günther, *Spectrochim. Acta, Part B*, 2001, **56**, 1219–1231.
- 22 J. van Elteren, S. Panighello, V. Šelih and E. Orsega, *Recent Advances in Laser Ablation ICP-MS for Archaeology*, 2016, pp. 53–71.
- 23 B. Wagner, A. Nowak, E. Bulska, J. Kunicki-Goldfinger, O. Schalm and K. Janssens, *Microchim. Acta*, 2008, **162**, 415–424.
- 24 M. Glascock, R. Speakman and R. Popelka-Filcoff, *Archaeological Chemistry. Analytical Techniques and Archaeological Interpretation*, 2007, vol. 968.
- 25 S. Cagnò, L. Favaretto, M. Mendera, A. Izmer, F. Vanhaecke and K. Janssens, *J. Archaeol. Sci.*, 2012, **39**, 1540–1552.
- 26 V. S. Šelih and J. T. Van Elteren, *Anal. Bioanal. Chem.*, 2011, **401**, 745–755.
- 27 J. T. Van Elteren, D. Metarapi, M. Šala, V. S. Šelih and C. C. Stremtan, *J. Anal. At. Spectrom.*, 2020, **35**, 2494–2497.
- 28 M. Šala, V. S. Šelih, C. C. Stremtan and J. Teun Van Elteren, *J. Anal. At. Spectrom.*, 2020, **35**, 1827–1831.
- 29 J. T. Van Elteren, V. S. Šelih and M. Šala, *J. Anal. At. Spectrom.*, 2019, **34**, 1919–1931.
- 30 A. Traviglia, S. Panighello, L. Moretto, E. Orsega, A. Bernardoni, S. Floreani, G. Moro and L. Mandruzzato, *presented in part at Annales du 21e Congrès Internationale pour l'Histoire du Verre, Istanbul*, September 2018.
- 31 J. T. Van Elteren, M. Šala and V. S. Šelih, *Anal. Chem.*, 2018, **90**, 5916–5922.
- 32 A. J. Mank and P. R. Mason, A Critical Assessment of Laser Ablation ICP-MS as an Analytical Tool for Depth Analysis in Silicabased Glass Samples, *J. Anal. At. Spectrom.*, 1999, **14**(8), 1143–1153.
- 33 H. Roemich, S. Gerlach, P. Mottner, F. Mees, P. Jacobs, D. Van Dyck and T. Doménech Carbó, *Mater. Res. Soc. Symp. Proc.*, 2003, **757**, 97–108.



34 A. Krauss, A. Whymark, A. Krauss and A. Whymark, *LPI*, 2021, 1489.

35 D. J. Huisman, S. Pols, I. Joosten, B. J. van Os and A. Smit, *J. Archaeol. Sci.*, 2008, **35**, 398–411.

36 M. G. Teresa Palomar and M.-A. V. Heras, *Coalition*, 2012, **23**, 2–6.

37 N. Schibille, P. Degryse, M. Corremans and C. G. Specht, *J. Archaeol. Sci.*, 2012, **39**, 1480–1492.

38 M. Truffa Giachet, B. Gratuze, S. Ozainne, A. Mayor and E. Huysecom, *J. Archaeol. Sci. Rep.*, 2019, **24**, 748–758.

39 B. Giussani, D. Monticelli and L. Rampazzi, *Anal. Chim. Acta*, 2009, **635**, 6–21.

40 T. Palomar, *Int. J. Appl. Glass Sci.*, 2017, **8**, 177–187.

41 T. Palomar and I. Llorente, *J. Non-Cryst. Solids*, 2016, **449**, 20–28.

42 O. Schalm and W. Anaf, *J. Non-Cryst. Solids*, 2016, **442**, 1–16.

43 C. Lenting, O. Plümper, M. Kilburn, P. Guagliardo, M. Klinkenberg and T. Geisler, *npj Mater. Degrad.*, 2018, **2**, 28.